Optical Beamforming Networks Supporting Multibeam and Multicast Operation

C. Tsokos[1], E. Andrianopoulos[1], A. Raptakis[1], N. Lyras[1], L. Gounaridis[1], P. Groumas[1,2], H. Avramopoulos[1], and Ch. Kouloumentas[1,2]

[1] National Technical University of Athens, 9 Iroon Polytechniou, Zografou 15773, Athens, Greece

[2] Optagon Photonics, Ag. Paraskevi 15341, Athens, Greece

Tel. +30-210-7722057, Email: ctso@mail.ntua.gr

ABSTRACT

In this paper, we validate the intrinsic capability of optical beamforming networks (OBFNs) to support simultaneously multi-beam and multicast operations. Through simulation analyses and assuming operation in the downlink direction of a wireless system, we verify the capability of an OBFN based on Blass-matrix architecture and an OBFN based on true-time delay (TTD) elements to support this hybrid mode of operation by calculating the radiation patterns and the resultant constellation diagrams of the demodulated signals at the corresponding observation angles. Finally, we experimentally assess the performance of a 1×4 TTD-OBFN based on commercially available components in the case of multicast operation. Using microwave signals at 15 GHz carrier frequency, high order modulation formats and 1 Gbaud symbol rates, we modulate the amplitude of a single optical carrier. After the processing of the modulated signals by the OBFN, we validate its potential to support multicast operation by calculating the BER of the received signals at the corresponding observation angles as a function of the optical power at the output of the OBFN. The BER remains below 10^{-3} for received optical power higher than -4 dBm, validating the potential of this OBFN architecture to support multicast operation.

Keywords: microwave photonics, beamforming, multicast, 5G, multi-beam operation, millimetre waves.

1. INTRODUCTION

Multicast beamforming has been a key feature enabling efficient wireless communication, not only in the traditional cellular networks, but also in the satellite communication systems [1], [2]. It has the ability to improve significantly the signal to interference plus noise ratio (SINR) of a wireless communication link, since it provides steered and highly directive radiation only to an interested group of terminals in contrast with the isotropic broadcasting. This also enables the compensation of the high propagation losses that are inherently met in the mmWave band, the frequency range where 5G networks are expected to be deployed. Furthermore, beamforming networks with the ability to support multi-beam operation are expected to play a key role in the emerging 5G networks, thanks to their ability to create multiple independent wireless links in a cellular system, vastly improving the total system capacity, whilst maintaining low cross-talk between the links. This can be beneficially implemented using optical beamforming networks, due to the immense scalability it offers in terms of bandwidth of operation, and the comparative low cost and power consumption, compared to the RF or digital counterpart beamforming solutions [3],[4].

In this paper, we validate through simulation analyses the capability of a Blass-matrix based optical beamforming network (OBFN) and an OBFN based on true-time delay (TTD) elements to operate concurrently in the multicast and the multi-beam mode. In addition, we experimentally evaluate the performance of an 1×4 TTD-OBFN when operating in the multicast mode by generating up to three beams, which are steered at different angles but carrying the same information signal.

2. THEORETICAL VALIDATION OF THE MULTI-BEAM AND MULTICAST OPERATION

The main goal of the simulation study performed in this work is to extend the capabilities of the optical beamforming network architectures proposed in [5], [6] so that they can also support multicast operation. In the context of the presented work, the operation of simultaneous transmission of multiple information signals in multiple angles (multi-beam and multicast operation) is referred to as the "hybrid operation". The two different architectures are presented in Fig. 1. These OBFNs are being evaluated respectively on the two following subsections. An inherent feature of the optical beamformers based on Blass-matrix architecture is their proneness to the beam squinting effect, which is related with the utilization of phase shifters. Due to this effect, different spectral components are steered to different angles which can lead to the deterioration of a wireless system's performance, especially when the signal bandwidth is very high, the antenna array is very long or the steering angles are highly deviating from the antenna boresight. In these cases, optical beamformers based on true-time delay (TTD) elements are selected due to their invulnerability to this effect.

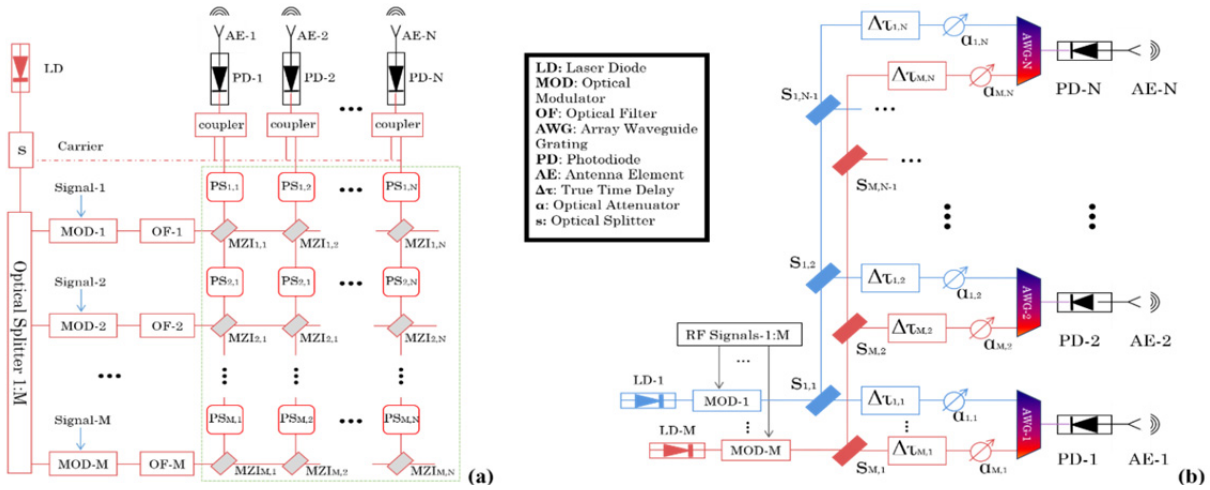

Figure 1. Layout of (a) an MxN Blass-matrix OBFN and (b) an MxN OBFN based on TTD elements.

2.1 Optical beamforming networks based on Blass-matrix architecture

The OBFNs based on the Blass-matrix architecture are on the research spotlight thanks to their capability to effectively handle multiple optical signals, each carrying a different information signal, and to generate the corresponding microwave beams by feeding an antenna array. The Blass-matrix consists of cross-connected horizontal and vertical waveguides using Mach-Zehnder interferometers (MZIs). The input optical signals are coupled to the OBFN via the horizontal waveguides and are split into multiple parts that follow different optical paths using the MZIs. The phase relationship between the optical paths is controlled using optical phase shifters that are connected to the one output port of each MZI. The vertical waveguides are connected to an array of photodiodes that detect the processed optical signals and generate the excitation signals driving the antenna array. Once the characteristics of each microwave beam are defined, the coupling coefficients of each MZI as well as the phase shifts induced by each optical phase shifter are tuned accordingly [5]. The preservation of the phase in the optical domain after the photodetection stage is possible when the input is an optical side-band signal and the optical carrier is reinserted before the photodetection process.

The capability of this OBFN to support hybrid operation is validated by simulating a 2×8 OBFN feeding a linear phased array (LPA) antenna consisting of 8 isotropic antenna elements (AEs). Within this simulation setup, we assume the simultaneous transmission of two wireless signals at 28.5 GHz carrier frequency with 1 Gbaud symbol rate. The first one, carrying 64-QAM modulation format is steered at 40° and 120° while the second one, carrying 16-QAM is steered at 90°. The effective bandwidth of both signals is limited using raised cosine pulse shaping filter with roll-off factor equal to 1. Side lobe suppression amplitude excitation schemes were used on the LPA, in order to reduce any interference between the transmitted beams. Specifically, the amplitude relationship between the excitation signals is dictated by a Gaussian distribution with standard deviation equal to 1.5.

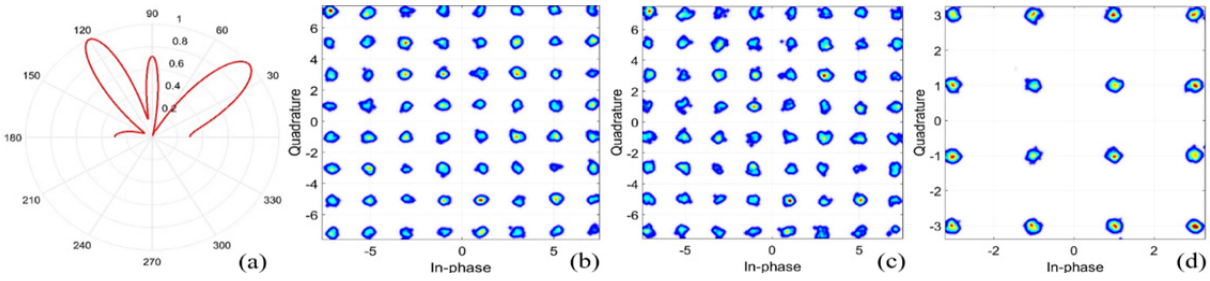

Figure 2. Simulation results of 2×8 Blass-matrix OBFN: (a) radiation pattern, (b) constellation diagram at 40°, (c) at 120°, (d) at 90°.

Based on the configuration algorithm presented in [5], and taking into account the above system specifications, we calculate the coupling coefficients of each MZI and the required phase shifts induced by each optical phase shifter. At the output ports of the Blass-matrix, the microwave signals feed the antenna array enabling the transmission over a radio-frequency (RF) channel based on an additive white Gaussian noise (AWGN) model. The SNR of both microwave signals is set at 28 dB. At the other end of the system, three different receivers consisting of a single isotropic AE are placed at the desired steering angles. Finally, the detected microwave signals are frequency down-converted to the baseband using a digital local oscillator at 28.5 GHz and are decoded. Figure 2 shows the calculated radiation pattern as well as the three resultant constellation diagrams at the corresponding steering angles. As it is observed, the results fully agree with the system's requirements and

more importantly, an error-free transmission is achieved, validating the potential of the OBFN to operate simultaneously in multicast and multi-beam operation.

2.2 Optical beamforming networks based on true-time delay elements

Following the same rationale as in the previous section, the capability of the optical beamformers based on TTD elements to support hybrid operation is validated by simulating a 2×8 OBFN. Two optical carriers are generated at different wavelengths and are coupled to two amplitude modulators. The modulators are driven by two microwave signals at 15 GHz carrier frequency with 1 Gbaud symbol rate, carrying a QPSK and a 16-QAM modulation format respectively. The spectra of the signals are shaped using raised cosine filters with roll-off factor equal to 1. The modulated signals are coupled to the OBFN which is based on optical splitters, optical TTD elements and variable optical attenuators (VOAs). Each input signal is split into eight different light paths using the optical splitters. These paths consist of a pair of a TTD element and a VOA, tuning the relative time-delay and amplitude relationships in accordance with the desired steering direction and the respective amplitude excitation scheme on the LPA.

In the scenario simulated, the QPSK signal is steered at 90° while the second signal carrying the 16-QAM modulation format is emitted at 50° and 140°. The amplitude excitation scheme used is dictated by the Chebyshev function with a major-to-minor lobe ratio of 30 dB. Finally, the output signals are detected by a photodiode array, and are transmitted by the LPA. The rest of the simulation setup remains the same as in the previous section, including the emulation of an RF channel based on an AWGN model and a single AE at each steering angle. The SNR of the wireless signals at the receiver is equal to 28 dB in all cases. After the frequency down-conversion and demodulation, the constellation diagrams are calculated. Figure 3 depicts the radiation pattern of the transmitter as well as the constellation diagram at each observation angle. As observed, an error-free transmission is achieved validating the potential of TTD based OBFNs to operate simultaneously in multicast and multi-beam operation.

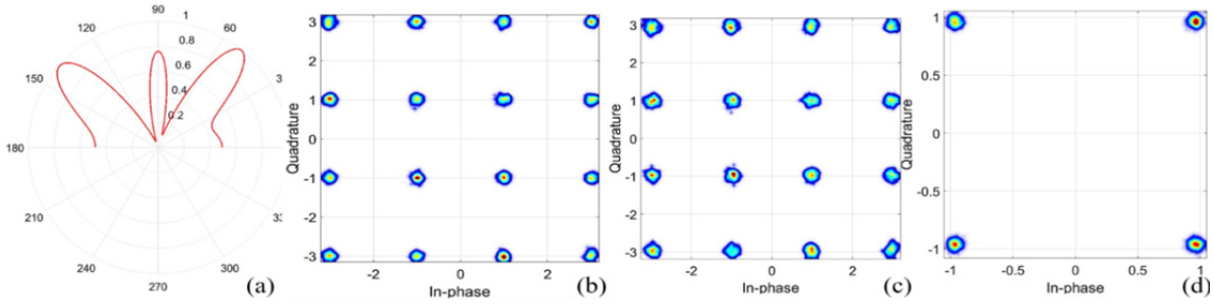

Figure 3. Simulation results of 2×8 TTD OBFN: (a) radiation pattern, (b) constellation diagram at 50°, (c) at 140°, (d) at 90°.

In order to provide continuity with the experimental study presented below, we repeat the same simulation study but with 4 AEs instead of 8. Figure 4 presents the calculated radiation pattern at the transmitter and the resultant constellation diagrams at the corresponding angles after the demodulation stage at the receivers. It becomes apparent that the reduction in the number of AEs leads to wider beam widths, thus creating inter-lobe interference. In our simulation, this interference can be easily observed between the beams steered at 90° and at 50° carrying a QPSK and a 16-QAM signal respectively.

Due to this interference, each original constellation point of the QPSK signal now consists of 16 different points, while on the other hand, each original constellation point of the 16-QAM signal consists now of 4 points arranged in the QPSK modulation format. Finally, the coexistence of multiple lobes transmitted by a smaller LPA, causes a deviation from the desired angle as can be observed in Fig. 4(a). This degradation is imposed on the system due to the LPA's incapability to create multiple radiation lobes independent with one another in a consistent manner when the number of the AEs are lower.

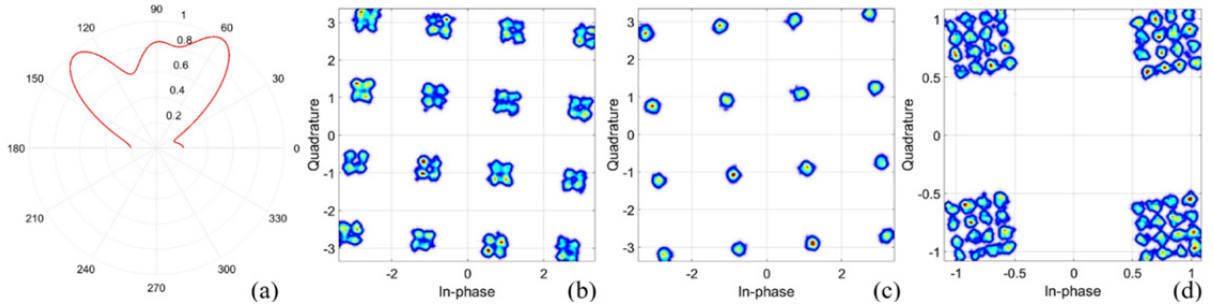

Figure 4. Simulation results of 2×4 TTD OBFN: (a) radiation pattern, (b) constellation diagram at 50°, (c) at 140°, (d) at 90°.

3. EXPERIMENTAL ANALYSIS

As already described in section 2, the Blass-matrix architecture requires a stable optical phase relationship between the optical signals in order to successfully control the characteristics of the emitted wireless beam. Therefore, for the implementation of this type of OBFNs, it is a prerequisite to use a photonic integration platform for the fabrication of compact circuits that can fulfill this stringent requirement [4]. On the other hand, OBFNs that deploy true-time delay elements for the handling of the optical signals can be developed using commercially available components. In this work, we validate the potential of the OBFNs to support multicast operation by developing an 1×4 TTD-OBFN, and experimentally evaluating its performance when operating in the downlink direction of a wireless system.

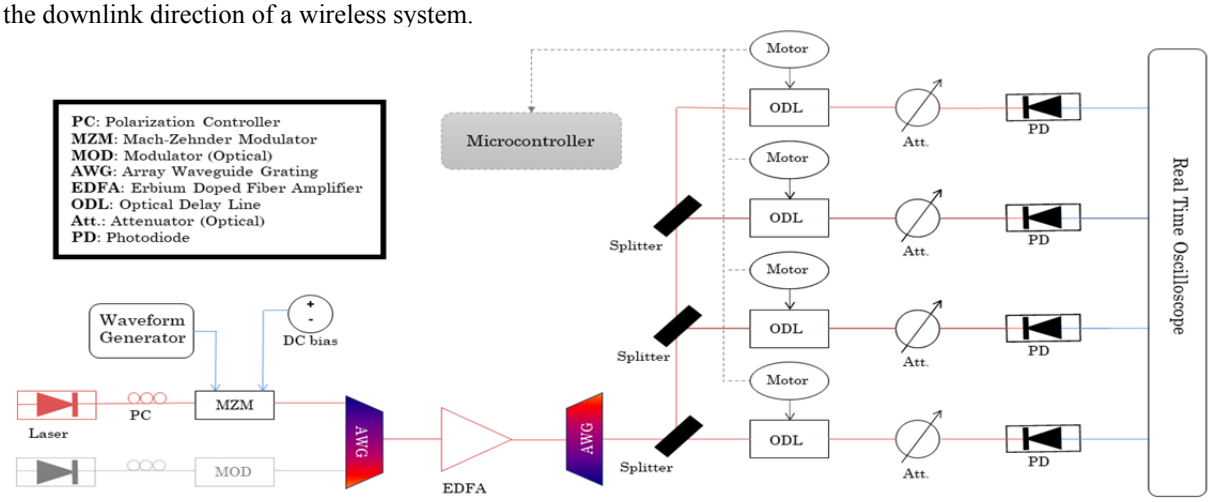

Figure 5. Experimental setup of an 1x4 TTD OBFN based on an array of ODLs and an array of VOAs.

Figure 5 depicts the corresponding experimental setup. A distributed feedback (DFB) laser generates a continuous wave optical carrier with central wavelength around 1558.17 nm. A 65 GSa/s arbitrary waveform generator generates microwave signals at 15 GHz carrier frequency, carrying modulation format either QPSK or 16-QAM with 1 Gbaud symbol rate. The signal's spectrum is limited using raised cosine pulse shaping filters with roll-off factor equal to 1. The microwave signal modulates the amplitude of the optical carrier using a Mach-Zehnder modulator (MZM). For the optimization of the amplitude modulation process, a polarization controller is placed at the path of the optical carrier, before the MZM. Subsequently, the modulated signal passes through an Erbium-doped fiber amplifier (EDFA), to compensate for the modulation losses and is coupled to the beamforming network. Using an array of three optical power splitters, the optical signal is split into four optical paths. In each path, a pair consisting of a tunable optical delay line (ODL) and a variable optical attenuator (VOA) is used to acquire the desired relative time delay and amplitude relationships. For ease of configuration, each ODL is mechanically connected to a programmable stepper motor controlled by a Raspberry Pi microcontroller. Therefore, the relative time delays are automatically set based on the desired steering angles. Finally, each signal is detected by the means of a single photodiode. The generated photocurrents are coupled to a 4-channel 80 GSa/s real time oscilloscope where they are sampled and stored for off-line processing. Specifically, the samples are used for the calculation of the resultant radiated field assuming operation of a 4-element LPA with isotropic AEs. The demodulation of the signals at each steering angle is based on a digital signal processing suite comprising of a frequency down-conversion unit, a low-pass filtering unit, a clock recovery unit, an amplitude level control unit, an equalization unit

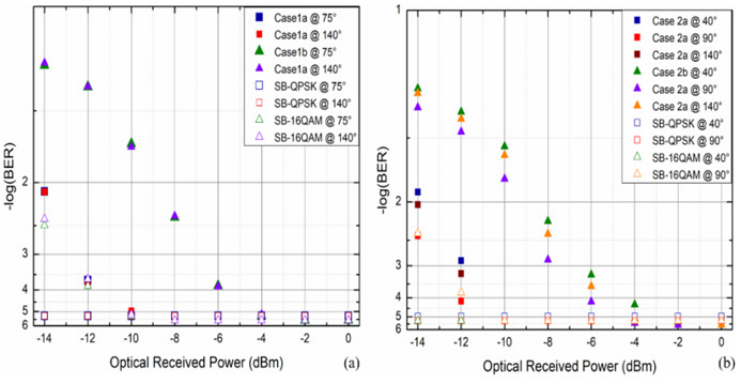

Figure 6. BER curves as a function of the ORP at the output of the OBFN.

Table 1. Experimental case-studies.

Case Index	Modulation Scheme	Transmission Angles
1a	QPSK	[75°, 140°]
1b	16-QAM	[75°, 140°]
2a	QPSK	[40°, 90°, 140°]
2b	16-QAM	[40°, 90°, 140°]

and a carrier recovery unit. The system evaluation is performed by calculating the BER over a set of eight million stored samples. Even though the same OBFN architecture can be modified accordingly to support the transmission of M different information signals (multi-beam or hybrid operation) using WDM elements for the generation and handling of the corresponding signals, the unavailability of more photodiodes limits our experimental study only in the case of the multicast operation. Table 1 outlines the cases that have been experimentally investigated summarizing the modulation format and the intended steering angles. Figure 6 summarizes the corresponding BER measurements for all cases with respect to the optical received power before the photodetection stage, as well as the reference BER measurements when each signal is transmitted individually to one steering angle (single-beam operation). As observed, in all cases the BER values remain below 10^{-3} for received optical power higher than -4 dBm, validating the potential of this OBFN architecture for multicast operation. Especially when transmitting a QPSK signal, the degradation imposed on the signal due to the coexistence of multiple beams remains negligible, validating the OBFN's proof of concept.

4. CONCLUSIONS

We validated through simulation analyses the potential of a Blass-matrix based OBFN and a TTD-OBFN to support simultaneously multicast and multi-beam mode operation. In addition, we experimentally evaluated the performance of an 1×4 TTD-OBFN, operating at the multicast mode with the ability to generate up to 3 different beams. In all cases the BER at the receiver remains lower than 10^{-3} when the ORP at the output of the OBFN remains higher than -4 dBm, validating the multicast operation.

REFERENCES

[1] G. Araniti, M. Condoluci, P. Scopelliti, A. Molinaro, and A. Iera, "Multicasting over emerging 5G networks: Challenges and perspectives", *IEEE Network*, vol. 31, no. 2, pp. 80-89, 2017.

[2] X. Zhang, S. Sun, F. Qi, R. Bo, R. Q. Hu, and Y. Qian, "Massive MIMO based hybrid unicast/multicast services for 5G," in *Proc. 2016 IEEE Global Communications Conference (GLOBECOM)*, Washington, DC, 2016.

[3] C. Roeloffzen *et al*., "Enhanced coverage though optical beamforming in fiber wireless networks," in *Proc. 2017 19th International Conference on Transparent Optical Networks (ICTON)*, Girona, 2017.

[4] C. Tsokos, P. Groumas, V. Katopodis, H. Avramopoulos, and C. Kouloumentas, "Enabling photonic integration technology for microwave photonics in 5G systems," in *Proc. 2017 19th International Conference on Transparent Optical Networks (ICTON)*, Girona, 2017.

[5] C. Tsokos *et al*., "Analysis of a multibeam optical beamforming network based on Blass matrix architecture," *Journal of Lightwave Technology*, vol. 36, no. 16, pp. 3354-3372, 15 Aug. 15, 2018.

[6] C. Tsokos, E. Mylonas, P. Groumas, L. Gounaridis, H. Avramopoulos, and C. Kouloumentas, "Optical beamforming network for multi-beam operation with continuous angle selection," *IEEE Photonics Technology Letters*, vol. 31, no. 2, pp. 177-180, 15 Jan.15, 2019.